analytical chemistry

pubs.acs.org/ac Article

Magnetic-Assisted Methylene Blue-Intercalated Amplified dsDNA for Polarity-Switching-Mode Photoelectrochemical Aptasensing

Fan Mo, Min Han, Xuan Weng, Yuye Zhang, Jing Li,* and Hongbo Li*

Cite This: *Anal. Chem.* 2021, 93, 1764−1770 Read Online

ACCESS | Metrics & More | Article Recommendations | Supporting Information

ABSTRACT: Organic dyes are typically applied as photosensitizers in photoelectrochemical (PEC) cells but have not been reported in polarity-reversal-mode PEC sensors with excellent sensitivity and accuracy. Herein, an elegant and robust PEC biosensor for carcinoembryonic antigen (CEA) has been designed by photocurrent polarity switching of CdTe quantum dots (QDs), which is obtained by embedding methylene blue (MB) into amplified double-stranded DNA (dsDNA) anchored to the superparamagnetic Fe_3O_4@SiO_2. The target-triggered Exo III-assisted cyclic amplification strategy and in situ magnetic enrichment enable the remarkable sensitivity. The extraction of target-analogue single-stranded DNA (output DNA) contributes to high selectivity resulting from the elimination of possible interferences in real samples or matrixes. Particularly, this exclusive polarity-reversal-mode PEC aptasensing can efficiently eliminate the false-positive or false-negative signals, leading to accurate measurements. Moreover, different from the probes and layer-by-layer assembled photoelectric beacons on electrodes in advance, this rational split-type approach is doomed to help the PEC biosensor with additional merits of convenient fabrication, short time consumption, wider linearity, as well as outstanding reproducibility and stability in practical applications. In light of the ability of MB acting as a kind of signal probe in typical electrochemical sensors, certainly, this ingenious design can not only be extended to a wide variety of target monitoring but also provide new ideas for the construction of high-performance electrochemical and PEC biosensors.

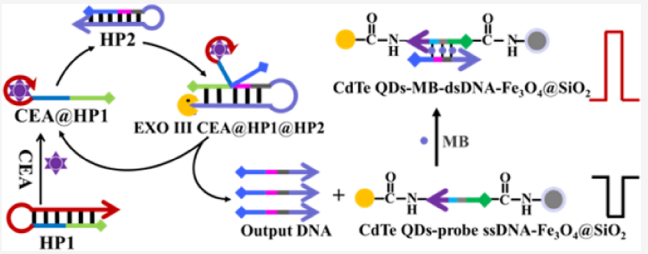

INTRODUCTION

In terms of biological signal amplification, several strategies, such as hybridization chain reaction (HCR),[1] catalytic hairpin assembly (CHA),[2] and rolling circle amplification (RCA)[3] have been proposed, and they are very effective for highly sensitive monitoring of biomolecules. In principle, these methods are related to strand displacement reactions and require the design of specific toehold-mediated dsDNA probes to facilitate the identification of DNA or RNA.[4] Alternatively, exonuclease-assisted cyclic amplification, as another forceful isothermal nucleic acid amplification strategy, can contribute to cumulate a large number of copies, leading to a convenient and efficient tool for the measurement of low-abundance biomolecules.[5] For example, λ-exonuclease,[6] exonuclease III (Exo III),[7] duplex-specific nuclease (DSN),[8] and T7 exonuclease (T7 Exo)[9] have all been introduced into PEC biosensors to facilitate signal amplification. Typically, as a sequence-independent enzyme, Exo III is capable of catalyzing the progressive digestion of dsDNA with blunt or recessed 3′ terminus but not dsDNA with protruding 3′-terminus or ssDNA.[10,11] During this process, the targets or target analogues are recovered, and numerous output DNAs are generated,[10] which can be hybridized to the complementary DNA modified with various signal transducers, such as electrochemistry,[11] fluorescence,[10] surface-enhanced Raman spectroscopy,[12] or photoelectrochemistry, for constructing DNA molecular machines.[13]

For more than a decade, photoelectrochemical (PEC) measurements have invoked amazing interest due to their ultra-sensitivity and simple instrument structure.[14] Up to now, in terms of signal expression types, almost all PEC sensors are focused on the construction of "signal-on"[15−17] or "signal-off"[18−20] modes. As is well known, the detection limit and sensitivity of the signal-off type PEC sensors are restricted by the high background noise,[8] let alone for their possibility of false-positive or false-negative detection results. Comparatively speaking, signal-on ones are beneficial to increase the sensitivity and accuracy, but they still face a serious challenge in eliminating false-positive or false-negative signals,[21] which are mainly rooted in the interference of coexisting oxidative or reductive species in complex real samples or detection matrix. Recently, a novel photocurrent polarity switching strategy has

Received: October 26, 2020
Accepted: December 16, 2020
Published: December 29, 2020

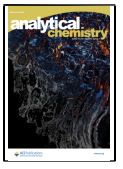

https://dx.doi.org/10.1021/acs.analchem.0c04521
Anal. Chem. 2021, 93, 1764−1770

Scheme 1. Schematic Illustration of the Exo III-Assisted Cyclic Amplification Signal (A) Reversal-Based PEC Aptasensor (B)

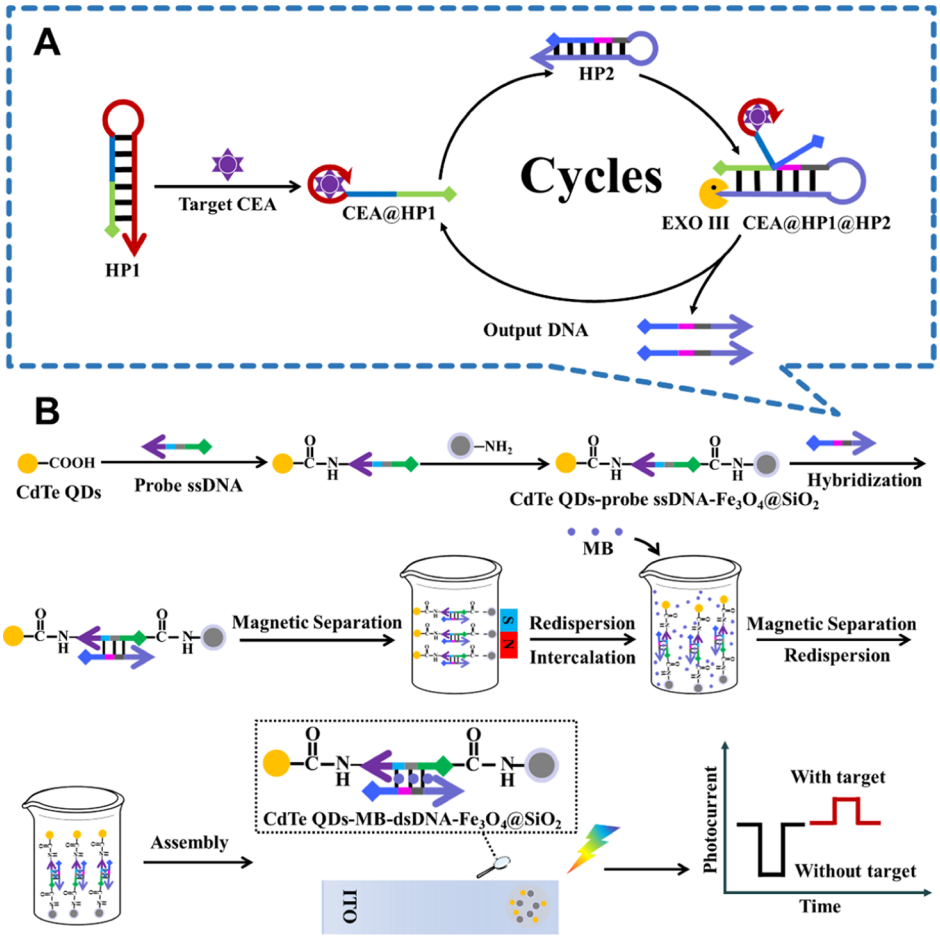

been reported by the introduction of a p-type Cu_2O−CuO semiconductor-based photoelectrode modified with n-type CdS quantum dots (QDs) in advance.[21] This novel strategy provides a new perspective for building a satisfactory PEC sensor. However, the polarity-switching-mode PEC aptasensor remains in its infancy. Additionally, so far, most of those reported PEC sensors were constructed by probes and layer-by-layer assembled photoelectric beacons on electrodes in advance. Such a fabrication approach is doomed to make PEC sensors with disadvantages of complex manufacturing process, long time consumption, limited selectivity, as well as poor reproducibility and stability, which may make the accuracy of test results difficult to meet the requirements of practical application. To address these shortcomings, we constructed a novel split-type and signal-on PEC aptasensor with excellent performance by introduction of superparamagnetic Fe_3O_4@SiO_2 particles.[22] As is well known, aptamer is a short chain of DNA or RNA that has high affinity to various targets. Obviously, it is very convenient to assemble the aptamer to DNA molecular machines for signal amplification. Consequently, combining DNA molecular machines, photocurrent polarity switching, and split-type mode is highly desirable for constructing general high-performance PEC biosensors.

In this work, an elegant and robust signal-reversal-mode PEC biosensor for carcinoembryonic antigen (CEA) was developed by intercalating methylene blue (MB) in magnified dsDNA connected to superparamagnetic Fe_3O_4@SiO_2 particles (Scheme 1). In the absence of CEA, the output DNA cannot be released and no dsDNA is formed or no MB is intercalated. Therefore, the photocathode current based on CdTe QD_S-probe ssDNA-Fe_3O_4@SiO_2 was obtained. However, upon exposure to CEA, Exo III can effectively catalyze the gradual digestion of CEA@HP1@HP2 to recycle CEA@HP1 and generate numerous output DNAs, which can be captured by CdTe QD_S-probe ssDNA-Fe_3O_4@SiO_2, and the resulting composite CdTe QD_S-dsDNA-Fe_3O_4@SiO_2 can be intercalated with MB and utilized for photocurrent detection. Surprisingly, the photoanode current was achieved under the same conditions. This photocurrent signal reversal can clearly indicate a certain concentration of CEA existing in real serum samples. Obviously, this amazing and remarkable signal polarity switching is greatly beneficial to advance the specificity and sensitivity of the PEC biosensor. Moreover, the superparamagnetic Fe_3O_4@SiO_2 enables the measurement of photocurrent to split from the CEA-triggered Exo III-assisted cyclic amplification system. This also contributes to enhance the specificity of the PEC biosensor by excluding the coexisting species in complex real samples. This distinctive working mechanism endues the PEC biosensor with additional merits of simple apparatus, easy operation, and short time consumption. This exclusive design will provide a new approach to high-performance PEC aptasensors for various analytes.

https://dx.doi.org/10.1021/acs.analchem.0c04521
Anal. Chem. 2021, 93, 1764−1770

EXPERIMENTAL SECTION

Assembly of CdTe QDs-Probe ssDNA-Fe_3O_4@SiO_2. First, 600 μL of prepared CdTe QDs was activated by 200 μL of ethyl(dimethylaminopropyl) carbodiimide (EDC) (100 mmol L^{-1}) and *N*-hydroxysuccinimide (NHS) (25 mmol L^{-1}) for 1 h at room temperature. Subsequently, 100 μL of probe ssDNA (10 μmol L^{-1}) was introduced and allowed to react at 37 °C for 6 h to generate CdTe QDs-probe ssDNA composites for following activation with EDC/NHS as above.[23] Then, 500 μL of the prepared Fe_3O_4@SiO_2-NH_2 suspension was diluted 10 times and 1 mL of the solution was added into the activated CdTe QDs-probe ssDNA suspension for 6 h at 37 °C to form CdTe QDs-probe ssDNA-Fe_3O_4@SiO_2 composites. They were then washed three times and extracted with the assistance of an external magnetic force. Subsequently, they were redispersed in 1 mL of buffer solution for following use. For photocurrent measurement, 20 μL of CdTe QDs-probe ssDNA-Fe_3O_4@SiO_2 composites was cast on a cleaned indium tin oxide (ITO) electrode and dried at 25 °C overnight, and the photocurrent response was obtained using the traditional three-electrode system in 0.1 mol L^{-1} phosphate-buffered saline (PBS, pH 7.0) solution at a bias voltage of 0.03 V with a chopped light irradiation.

Enzyme-Assisted Biological Signal Amplification. First, 50 μL of 10 μmol L^{-1} hairpin-structured HP1 and HP2 solutions were heated to 95 °C for 3 min, respectively. Then, their stable structures formed when the temperature gradually decreased to 25 °C.[24] After that, 5.0 μL of CEA at various concentrations was individually added into 45 μL of the solution containing 1.0 μmol L^{-1} HP1, 2.0 μmol L^{-1} HP2, and 20 U Exo III. Then, they were heated at 37 °C for 1 h to carry out the Exo III-assisted cyclic amplification (Figure S1).[10] To end the enzymatic reaction, the temperature was further increased to 70 °C and kept for 10 min.

Construction of PEC Biosensing Platforms. First, 100 μL of CdTe QDs-probe ssDNA-Fe_3O_4@SiO_2 suspension was scattered into the above Exo III-assisted cyclic amplification system and heated to 37 °C for 2 h.[25] Then, the released output DNA was captured by CdTe QDs-probe ssDNA-Fe_3O_4@SiO_2 to form CdTe QDs-dsDNA-Fe_3O_4@SiO_2 composites. Further, the composites were extracted and redispersed in 50 μL of buffer solution, and then 50 μL of 1 mmol L^{-1} MB solution was introduced for intercalation. Five minutes later, the resulting CdTe QDs-MB-dsDNA-Fe_3O_4@SiO_2 composites were extracted with an external magnetic force, washed three times, and rescattered in 100 μL of buffer solution. At last, 20 μL of the solution was utilized for ITO electrode modification. After drying at 25 °C overnight, the prepared PEC aptasensor was implemented to collect photocurrent in PBS (0.1 mol L^{-1}, pH 7.0) solution at a bias potential of 0.03 V in response to a chopped light irradiation.

RESULTS AND DISCUSSION

Material Characterization. The morphologies and structures of the prepared function materials were imaged by high-resolution transmission electron microscopy (HRTEM). As shown in Figure 1A–C, the size of CdTe QDs is approximately 3 nm. Figure 1B shows the uniform and monodisperse core–shell structured Fe_3O_4@SiO_2 with a total size of ~170 nm in diameter. To prove the successful preparation of CdTe QDs and Fe_3O_4@SiO_2 particles, they were further validated by X-ray diffraction (XRD). The orange

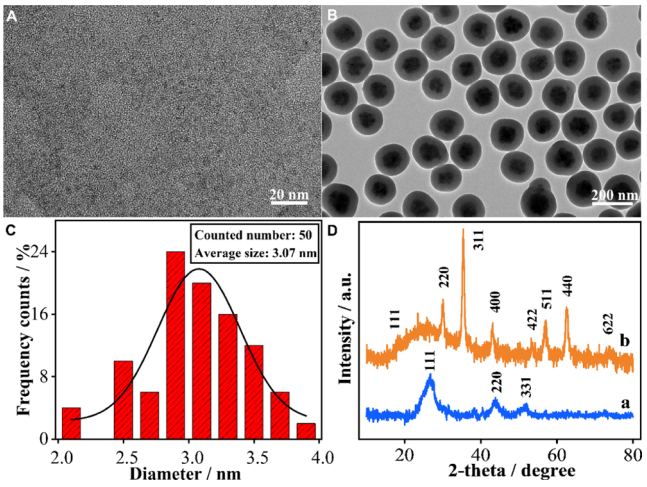

Figure 1. HRTEM images of CdTe QDs (A), Fe_3O_4@SiO_2 particles (B), and (D) the XRD of CdTe QDs (a) and Fe_3O_4@SiO_2 particles (b). (C) Selected particle size statistics of CdTe QDs in (A).

curve in Figure 1D represents the XRD pattern of Fe_3O_4@SiO_2, in which the wide peak located at 22.5° is consistent with that of colloidal SiO_2 (JCPDS 29-0085). The additional typical diffraction peaks at 18.3° (111), 30.1° (220), 35.4° (311), 43.1° (400), 53.4° (422), 56.9° (511), 62.5° (440), and 74.9° (622) are well consistent with the magnetite Fe_3O_4 phase (JCPDS 19-0629). This indicates that Fe_3O_4@SiO_2 particles were obtained.[19] Also, the blue curve exhibits wide peak patterns located at 26.70, 43.80, and 51.60°, which can be ascribed to the (111), (220), and (311) planes of CdTe QDs,[26] indicating that the CdTe QDs were achieved.

Polyacrylamide Gel Electrophoresis (PAGE) Characterization. Native polyacrylamide gel electrophoresis (PAGE) was used to demonstrate the Exo III-assisted biological signal amplification process. In the entire signal amplification system, the hairpin-structured HP1 and HP2 were precisely designed. As shown in Figure 2, lane 1 and lane 2 individually show the profiles of HP1 and HP2, indicating that there is no spontaneous interaction with each other when the target does not exist. When Exo III was introduced into equivalent amounts of HP1 and HP2, two bands are clearly displayed in lane 3 to indicate that HP1 and HP2 are not paired. However, when CEA was added into the equal amounts of HP1 and HP2, there is a new band appearing at the top of lane 4, suggesting that the CEA@HP1@HP2 composite was generated. Further, when Exo III was introduced into the composites, the band of the CEA@HP1@HP2 composite disappeared, indicating that Exon III can gradually digest CEA@HP1@HP2 to recycle CEA@HP1 and generate a large amount of single-stranded output DNA, which was not shown in lane 5 because the single-strand structure cannot be intercalated with ethidium bromide (EB). The strand locations in lanes 1–5 are consistent with those of the DNA marker in lane M. Therefore, Exo III-assisted cyclic amplification strategy has been successfully proved, and it can be applied to the highly sensitive measurement of CEA.

Electrode Assembly Characterization. To confirm the successful assembly of the CdTe QDs-MB-dsDNA-Fe_3O_4@SiO_2 composite, electrochemical impedance spectroscopy (EIS) was utilized to investigate the electrode modification in sequence. As shown in the Nyquist plots (curves a–d, Figure 3A), the semicircle diameters corresponding to the

https://dx.doi.org/10.1021/acs.analchem.0c04521
Anal. Chem. 2021, 93, 1764–1770

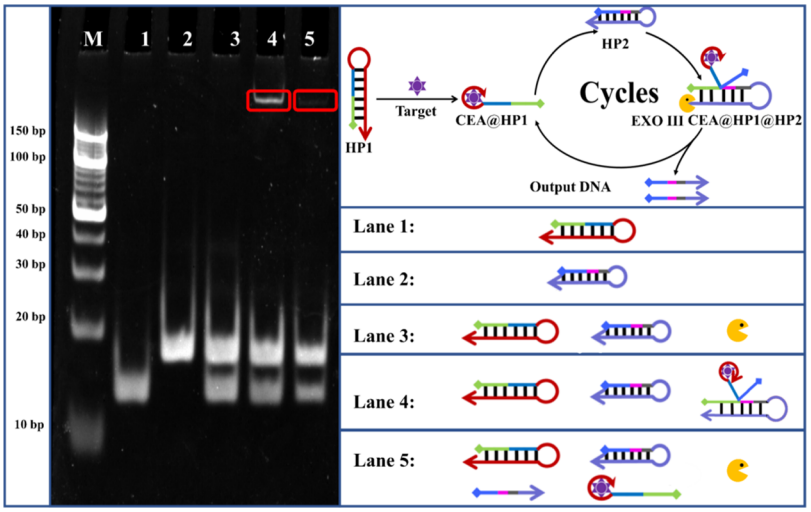

Figure 2. Native PAGE characterization for the Exo III-assisted cyclic amplification strategy. Lane M: DNA marker (10−150 bp); lane 1: H1 (10 μL, 10 μmol L^{-1}); lane 2: H2 (10 μL, 10 μmol L^{-1}); lane 3: H1 + H2 (10 μL, 10 μmol L^{-1}) + Exo III (20 U); lane 4: HP1 + HP2 (10 μL, 10 μmol L^{-1}) + CEA (0.5 μL, 0.1 ng mL^{-1}); and lane 5: H1 + H2 (10 μL, 10 μmol L^{-1}) + CEA (0.5 μL, 0.1 ng mL^{-1}) + Exo III (20 U).

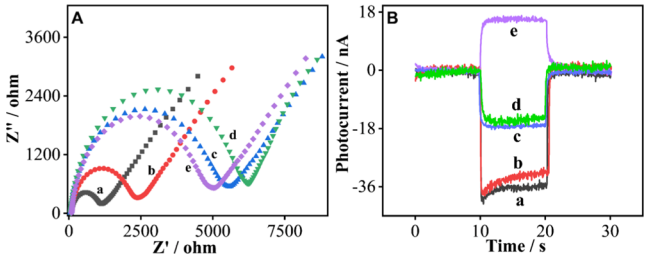

Figure 3. (A) Nyquist plots of modified glassy carbon electrodes with CdTe QDs (a), CdTe QDs-probe ssDNA (b), CdTe QDs-probe ssDNA-Fe_3O_4@SiO_2 (c), CdTe QDs-dsDNA-Fe_3O_4@SiO_2 (d), and CdTe QDs-MB-dsDNA-Fe_3O_4@SiO_2 (e) in 2.5 mmol L^{-1} $K_4Fe(CN)_6$ and $K_3Fe(CN)_6$. (B) Corresponding materials modified on ITO electrodes for photocurrent measurements.

charge-transfer resistance (R_{ct}) values increase in turn, suggesting that CdTe QDs (curve a) have been successfully assembled with probe ssDNA (curve b), Fe_3O_4@SiO_2 (curve c), and output DNA (curve d). These magnified R_{ct} values come from the modified species that effectively prevent electron transfer of the negative-charged redox probes in light of the anionic polymer property of DNA biomoleculars or the insulator SiO_2. After the intercalation of MB, however, the R_{ct} value of curve e reduced compared to that of curve d. It benefits from the electroactive MB.[27,28] These indicate that the CdTe QDs-MB-dsDNA-Fe_3O_4@SiO_2 composite was achieved by the assembly in order.

To further assess the successful modification of the corresponding material, photocurrent measurements were also performed. As shown in Figure 3B, compared to the CdTe QD-based photocathode current of 36.5 nA (curve a), curve b exhibited a slight decrease in photocurrent when probe ssDNA was modified on CdTe QDs. When they were further assembled onto the nonconductive Fe_3O_4@SiO_2 particles, a remarkably decreased photocurrent of 18.2 nA is shown in

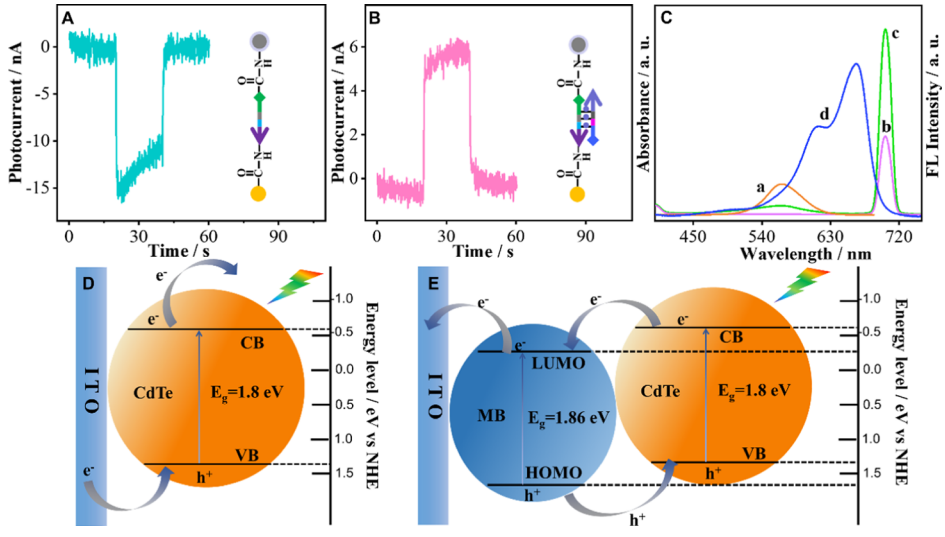

Figure 4. CdTe QD_S-probe ssDNA-Fe_3O_4@SiO_2-based photoelectric response and its working mechanism (A, D), and 10 fg mL^{-1} CEA-triggered Exo III-assisted cyclic amplification signal reversal and its working principle (B, E). (C) Fluorescence spectra of CdTe QDs (a), MB (b), CdTe QDs-MB-dsDNA-Fe_3O_4@SiO_2 (c) (λ_{ex} = 350 nm), and the UV−visible spectrum of MB (d).

https://dx.doi.org/10.1021/acs.analchem.0c04521
Anal. Chem. 2021, 93, 1764−1770

curve (c). After forming dsDNA with output DNAs, curve d exhibits a slightly lower photocurrent compared with that of curve c. However, when MB was intercalated into the dsDNA, the polarity-switched photocurrent response was obtained (curve e) at the same bias potential of 0.03 V. These further confirm the formation of the CdTe QDs-MB-dsDNA-Fe_3O_4@SiO_2 composite. Also, this phenomenon of photocurrent polarity switching lays a foundation for PEC analysis.

Amplified Signal-Reversal PEC Biosensor and Its Working Mechanism. Exo III-assisted cyclic amplification strategy combined with superparamagnetic Fe_3O_4@SiO_2 was utilized to build a signal polarity-switched-mode CEA PEC biosensor (Scheme 1). In the absence of CEA, base pairing cannot be formed spontaneously between HP1 and HP2. Also, the unpaired single base at the end of HP1 and HP2 can efficiently prevent Exo III from cleaving. Consequently, the output DNA cannot be released and thus the extracted CdTe QD_S-probe ssDNA-Fe_3O_4@SiO_2 composite cannot be intercalated with MB. Consequently, the photocathode current was obtained in view of the p-type semiconductor property of CdTe QDs (Figure 4A). Upon exposure to CEA, the hairpin-structured HP1 was unfolded to emerge the CEA@HP1 structure since a part of its sequence was ingeniously designed as the aptamer of CEA. Then, the exposed portion of HP1 would complement the toehold of HP2 to form the CEA@HP1@HP2 structure. Subsequently, Exo III can cleave the blunt end of CEA@HP1@HP2 along the 3′ to 5′[10,29] to recycle CEA@HP1 and release the single-stranded output DNA, which can be captured by probe ssDNA to form the composite CdTe QD_S-dsDNA-Fe_3O_4@SiO_2. After magnetic separation, the extracted composite CdTe QD_S-dsDNA-Fe_3O_4@SiO_2 can be intercalated with MB for the photocurrent detection with opposite polarity (Figure 4B). Therefore, the flat-structured MB as an intercalator has played a significant role in the realization of PEC signal reversal. As could be seen from Figure 4C, compared to the single fluorescence emission of CdTe QDs at 562 nm (curve a) and MB at 698 nm (curve b), the fluorescence of the composite CdTe QD_S-MB-dsDNA-Fe_3O_4@SiO_2 was the result of fluorescence quenching of CdTe QDs and the enhancement of MB (curve c). The former quenching could be explained by the band alignment between CdTe QDs and MB, which provides a facile channel of photogenerated electron transfer. This could also be seen from the photocurrent polarity reversal as mentioned above. However, compared to the fluorescence of MB in solution, the latter fluorescence enhancement of MB intercalated into dsDNA could be explained by the aggregation-induced emission or the adjacent resonance energy transfer from CdTe QDs, both of them enhancing the absorption of MB and then the fluorescence emission. These spectral features indicate that the photogenerated electrons of CdTe QDs can be injected into the lowest unoccupied molecular orbital (LUMO) of MB, and then more electrons can transfer to the ITO electrode at a bias voltage of 0.03 V. To demonstrate the working mechanism, the conduction band (E_{CB}, −0.52 eV) and valence band (E_{VB}, 1.28 eV) of CdTe QDs have been calculated in our recent work.[30] Also, the LUMO and highest occupied molecular orbital (HOMO) of MB are −4.25 and −6.11 eV (vs vacuum), respectively.[31] As a result, the LUMO and HOMO of MB can be calculated as −0.25 and 1.61 eV (vs NHE) by the following eq 1.[32]

$$E_{\text{vs NHE}} = -4.5 - E_{\text{vs vacuum}} \quad (1)$$

As shown in Figure 4D, by transferring electrons to PBS through an external circuit, the CdTe QD_S-probe ssDNA-Fe_3O_4@SiO_2-based ITO electrode exhibits a photocathode current of 17.5 nA. However, after MB intercalation, the CdTe QD_S-MB-dsDNA-Fe_3O_4@SiO_2-based ITO electrode reveals an opposite polarity photocurrent of 6.5 nA under the same condition. The direction of the electron transfer can be proposed that it is from CB of CdTe QDs to LUMO of MB and then to the external circuit (Figure 4E). Herein, the rational and matched energy band levels between CdTe QD_S and MB contribute to the photocurrent polarity reversal. Moreover, MB intercalated in the rigid dsDNA shortens the electron transmission path, further enhancing the photoanode signal. As far as we know, MB-induced PEC sensing signal reversal has not been reported. Also, it is different from the sensitized effect of MB for the signal-on type[9] and ratiometric PEC sensors.[33,34]

Analytical Performance of As-Designed PEC Aptasensor. The measurement of CEA is through the signal-reversal PEC biosensing platform constructed by Exo III-assisted cyclic amplification strategy combined with functionalized superparamagnetic Fe_3O_4@SiO_2 particles. By the trigger of various concentrations of CEA, large amounts of output DNAs would be released and they can be captured by the composite CdTe QDs-probe ssDNA-Fe_3O_4@SiO_2. With the help of magnetic separation, the resulting composite CdTe QDs-dsDNA-Fe_3O_4@SiO_2 was formed and could be intercalated with MB, and then they were utilized for electrode assembly and photocurrent measurement (Figure 5A). As

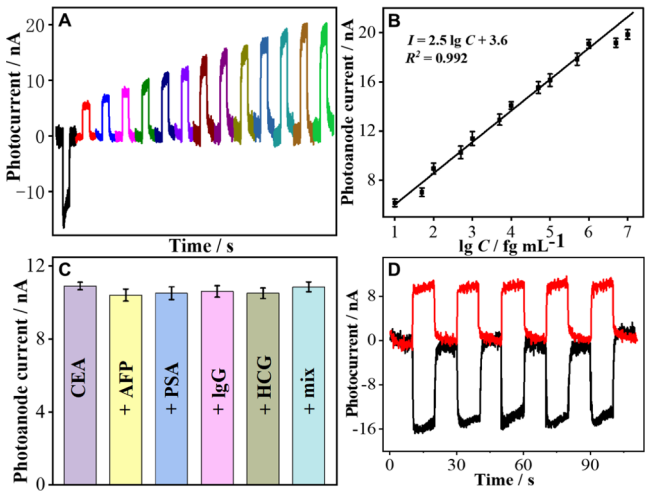

Figure 5. (A) Photocurrent responses of the PEC biosensor in 0.1 mol L^{-1} PBS (pH 7.0) containing 0, 10, 50, 100, 500 fg mL^{-1}; 1, 5, 10, 50, 100, 500 pg mL^{-1}; and 1, 5, 10 ng mL^{-1} CEA. (B) Linear calibration curve. (C) Interference investigation by conventional proteins such as human chorionic gonadotropin (HCG), α-feto-protein (AFP), prostate-specific antigen (PSA), and immunoglobulin G (IgG), and a mixture of each of the above. (D) Time-based typical photocurrent of the PEC biosensor in 0.1 mol L^{-1} PBS (pH 7.0) containing 0 and 500 fg mL^{-1} CEA.

shown, the photocurrent for the signal-reversal PEC response gradually enhances as the concentration of CEA increases. Obviously, we can take no account of the photocurrent for the background photocathode response, and thus obtain a PEC biosensor with a real zero-background signal, further extremely improving the detection sensitivity. The reversed anode

https://dx.doi.org/10.1021/acs.analchem.0c04521
Anal. Chem. 2021, 93, 1764−1770

Table 1. Different Detection Methods for CEA

method	linear range	LOD	references
electrochemiluminescence	10 pg mL^{-1} to 125 ng mL^{-1}	3 pg mL^{-1}	35
electrochemiluminescence	30 pg mL^{-1} to 6 ng mL^{-1}	5.38 pg mL^{-1}	36
fluorescence	0.1 pg mL^{-1} to 10 ng mL^{-1}	0.065 pg mL^{-1}	23
colorimetric	5 pg mL^{-1} to 10 ng mL^{-1}	0.5 pg mL^{-1}	37
thermometers	7.81 pg mL^{-1} to 500 pg mL^{-1}	0.6 pg mL^{-1}	38
PEC	10 pg mL^{-1} to 5 ng mL^{-1}	4.8 pg mL^{-1}	39
PEC	5 pg mL^{-1} to 5 ng mL^{-1}	1.9 pg mL^{-1}	40
PEC	1 fg mL^{-1} to 1 ng mL^{-1}	0.46 fg mL^{-1}	13
PEC	10 fg mL^{-1} to 1 ng mL^{-1}	3.98 fg mL^{-1}	this work

photocurrent for the resulting PEC aptasensor exhibited an expanded linear range with the concentration of CEA from 10 fg mL^{-1} to 1 ng mL^{-1} (Figure 5B), and the detection limit of 3.98 fg mL^{-1} was worked out at 3S/N. Such a low detection limit has an advantage over most other detection methods (Table 1). Ultra-sensitivity is mainly attributed to the Exo III-assisted cyclic amplification strategy, magnetic enrichment, and signal-reversal mode. Also, the as-designed signal-reversal-mode PEC biosensor has other merits such as simple apparatus, easy operation, and short time consumption.

The specificity of the polarity-reversal PEC aptasensor was evaluated by introducing conventional biomarkers in 1 pg mL^{-1} CEA (Figure 5C). Upon exposure to coexisting species, the change in photocurrent was less than 5%, indicating that 100 pg mL^{-1} human chorionic gonadotropin (HCG), α-fetoprotein (AFP), prostate-specific antigen (PSA), immunoglobulin G (IgG), and 10 pg mL^{-1} each of the above coexisting species do not interfere with the measurement of CEA. The excellent selectivity of the as-designed PEC biosensor can be attributed to the selective recognition of CEA aptamers, magnetic separation of functionalized superparamagnetic Fe_3O_4@SiO_2 particles, and the significant polarity reversal mode.[41−44]

The stability of the signal-reversal-mode PEC biosensor was assessed by five consecutive photoexcitation cycles (Figure 5D). Specifically, in the presence of 500 fg mL^{-1} CEA, the output DNA can be liberated from HP2. Then, the resulting composite CdTe QDs-dsDNA-Fe_3O_4@SiO_2 was extracted from the target-triggered Exo III-assisted cyclic amplification system. After washing treatment and MB intercalation, the resulting composite CdTe QDs-MB-dsDNA-Fe_3O_4@SiO_2 was extracted and redispersed in 100 μL of buffer solution. Subsequently, 20 μL of the above composite was cast on a cleaned ITO electrode and dried at 25 °C overnight. Then, it was used for photocurrent measurement at a bias of 0.03 V with a chopped light irradiation over 110 s. However, in the absence of CEA (0 fg mL^{-1}), only the composite CdTe QDs-probe ssDNA-Fe_3O_4@SiO_2 was extracted. As shown in Figure 5D, there is little change in both the photocurrent responses. Moreover, the long-term stability was evaluated by weekly photocurrent measurements. When the PEC sensors were not in use, they were stored at 4 °C in a refrigerator. The photoelectric response was almost consistent with the initial value in 2 weeks, and even after 4 weeks, it still maintained 93.7% of the original value (Figure S2). This suggests that the PEC biosensor possesses a satisfactory stability. In addition, reproducibility was estimated by the calibration curves of the six freshly prepared PEC biosensors (Figure 5B). As shown, the relative standard deviation (RSD) was no more than 4.7%, indicating the PEC biosensor can be reproduced.

CEA standards of various concentrations were added to real human serum samples to evaluate the feasibility of PEC sensors in practical applications. As shown in Figure S3 and Table 2, the recovery of the PEC biosensor is between 97.9 and 105.1% and the RSD is less than 3.98%, suggesting that the PEC aptasensor has potential in clinical application.

Table 2. Determination of CEA in Human Serum Samples by the Proposed PEC Biosensor

sample	added (fg mL^{-1})	found (fg mL^{-1})	recovery (%)	RSD (%)
human serum	0	10.2		1.36
	100	115.3	105.1	2.83
	500	501.2	98.2	2.56
	1000	989.6	97.9	3.98

CONCLUSIONS

Altogether, a novel signal polarity-reversed PEC aptasensor for CEA as a model was constructed via intercalation of MB into CdTe QD_S-dsDNA-Fe_3O_4@SiO_2 composites. The target-triggered Exo III-assisted target-analogue cyclic amplification strategy has been evaluated by PAGE characterization and helps improving the PEC sensitivity. Also, the prepared superparamagnetic Fe_3O_4@SiO_2 particles have been functionalized with CdTe QD_S-tagged probe ssDNA and then were successfully utilized to capture a large number of released output DNAs. With the assistance of magnetic extraction and enrichment, the resulting CdTe QD_S-dsDNA-Fe_3O_4@SiO_2 composites were intercalated with MB, which made the signal polarity of CdTe QDs reverse. The working mechanism of photocurrent signal reversal by MB was discussed in detail with the help of a band diagram and fluorescence spectra. This unique and rational design remarkably enhanced the detection sensitivity. In particular, this exclusive signal-reversal mode combined with superparamagnetic Fe_3O_4@SiO_2 particles contributes to greatly boost the selectivity by eliminating the false signals and removing the potential interferents from the modified electrodes. Also, the linear range of 5 orders of magnitude benefits from a large amount of released output DNAs and the enrichment of functionalized superparamagnetic Fe_3O_4@SiO_2 particles. In addition, this signal-reversal-mode PEC biosensor shows merits of simple apparatus, easy operation, less time consuming, as well as excellent reproducibility and stability in practical settings. Given the redox properties of the flat structure of MB and its ability to insert dsDNA, this exquisite design opens up new perspectives for the construction of high-performance electrochemical or PEC biosensors.

https://dx.doi.org/10.1021/acs.analchem.0c04521
Anal. Chem. 2021, 93, 1764−1770

■ ASSOCIATED CONTENT

Supporting Information

The Supporting Information is available free of charge at https://pubs.acs.org/doi/10.1021/acs.analchem.0c04521.

Reagents, apparatus, synthesis of Fe_3O_4@SiO_2-NH_2 particles and CdTe QDs, impedance measurements, gel electrophoresis characterization, and incubation time optimization (PDF)

■ AUTHOR INFORMATION

Corresponding Authors

Jing Li − *School of Chemistry and Chemical Engineering, Yancheng Institute of Technology, Yancheng 224051, P. R. China*; Email: jli@ycit.edu.cn

Hongbo Li − *School of Chemistry and Chemical Engineering, Yancheng Institute of Technology, Yancheng 224051, P. R. China*; Phone: +86-515-88298735; Email: hbli@ycit.edu.cn

Authors

Fan Mo − *School of Chemistry and Chemical Engineering, Yancheng Institute of Technology, Yancheng 224051, P. R. China*

Min Han − *School of Chemistry and Chemical Engineering, Yancheng Institute of Technology, Yancheng 224051, P. R. China*

Xuan Weng − *School of Chemistry and Chemical Engineering, Yancheng Institute of Technology, Yancheng 224051, P. R. China*

Yuye Zhang − *School of Chemistry and Chemical Engineering, Yancheng Institute of Technology, Yancheng 224051, P. R. China*

Complete contact information is available at: https://pubs.acs.org/10.1021/acs.analchem.0c04521

Notes

The authors declare no competing financial interest.

■ ACKNOWLEDGMENTS

We acknowledge the financial support from the Natural Science Foundation of China (21505117 and 21775135) and the Natural Science Foundation of Jiangsu Province (BK20161309 and BK20201473), and this work was also sponsored by Qinglan Project of Jiangsu Province.

■ REFERENCES

(1) Figg, C. A.; Winegar, P. H.; Hayes, O. G.; Mirkin, C. A. *J. Am. Chem. Soc.* **2020**, *142*, 8596−8601.

(2) Karunanayake Mudiyanselage, A. P. K. K.; Yu, Q.; Leon-Duque, M. A.; Zhao, B.; Wu, R.; You, M. *J. Am. Chem. Soc.* **2018**, *140*, 8739−8745.

(3) Shen, C.; Liu, S.; Li, X.; Yang, M. *Anal. Chem.* **2019**, *91*, 11614−11619.

(4) Simmel, F. C.; Yurke, B.; Singh, H. R. *Chem. Rev.* **2019**, *119*, 6326−6369.

(5) Wen, S.; Su, Y.; Dai, C.; Jia, J.; Fan, G. C.; Jiang, L. P.; Song, R. B.; Zhu, J. J. *Anal. Chem.* **2019**, *91*, 12298−12306.

(6) Zhang, K.; Lv, S.; Tang, D. *Anal. Chem.* **2019**, *91*, 10049−10055.

(7) Gao, X.; Cai, Q.; Li, H.; Jie, G. *Anal. Chem.* **2020**, *92*, 6734−6740.

(8) Li, M.; Xiong, C.; Zheng, Y.; Liang, W.; Yuan, R.; Chai, Y. *Anal. Chem.* **2018**, *90*, 8211−8216.

(9) Hou, T.; Xu, N.; Wang, W.; Ge, L.; Li, F. *Anal. Chem.* **2018**, *90*, 9591−9597.

(10) He, M. Q.; Wang, K.; Wang, W. J.; Yu, Y. L.; Wang, J. H. *Anal. Chem.* **2017**, *89*, 9292−9298.

(11) Liu, S.; Wang, C.; Zhang, C.; Wang, Y.; Tang, B. *Anal. Chem.* **2013**, *85*, 2282−2288.

(12) Zhou, W.; Tian, Y. F.; Yin, B. C.; Ye, B. C. *Anal. Chem.* **2017**, *89*, 6120−6128.

(13) Zhang, Y. H.; Li, M. J.; Wang, H. J.; Yuan, R.; Wei, S. P. *Anal. Chem.* **2019**, *91*, 10864−10869.

(14) Shu, J.; Tang, D. *Anal. Chem.* **2020**, *92*, 363−377.

(15) Zhao, C. Q.; Zhou, J.; Wu, K. W.; Ding, S. N.; Xu, J. J.; Chen, H. Y. *Anal. Chem.* **2020**, *92*, 6886−6892.

(16) Wang, S.; Wang, F.; Fu, C.; Sun, Y.; Zhao, J.; Li, N.; Liu, Y.; Ge, S.; Yu, J. *Anal. Chem.* **2020**, *92*, 7604−7611.

(17) Lv, S.; Zhang, K.; Zhu, L.; Tang, D. *Anal. Chem.* **2020**, *92*, 1470−1476.

(18) Zhou, Q.; Li, G.; Chen, K.; Yang, H.; Yang, M.; Zhang, Y.; Wan, Y.; Shen, Y.; Zhang, Y. *Anal. Chem.* **2020**, *92*, 983−990.

(19) Li, H.; Li, Y.; Li, J.; Yang, F.; Xu, L.; Wang, W.; Yao, X.; Yin, Y. *Anal. Chem.* **2020**, *92*, 4094−4100.

(20) Hu, D.; Liang, H.; Wang, X.; Luo, F.; Qiu, B.; Lin, Z.; Wang, J. *Anal. Chem.* **2020**, *92*, 10114−10120.

(21) Fu, Y.; Zou, K.; Liu, M.; Zhang, X.; Du, C.; Chen, J. *Anal. Chem.* **2020**, *92*, 1189−1196.

(22) Li, J.; Xu, L.; Shen, Y.; Guo, L.; Yin, H.; Fang, X.; Yang, Z.; Xu, Q.; Li, H. *Anal. Chem.* **2020**, *92*, 8607−8613.

(23) Jie, G.; Li, C.; Zhao, Y.; Kuang, Q.; Niu, S. *ACS Appl. Nano Mater.* **2019**, *2*, 4637−4645.

(24) Ge, L.; Wang, W.; Sun, X.; Hou, T.; Li, F. *Anal. Chem.* **2016**, *88*, 2212−2219.

(25) Xu, Z. H.; Wang, H.; Wang, J.; Zhao, W.; Xu, J. J.; Chen, H. Y. *Anal. Chem.* **2019**, *91*, 12000−12005.

(26) Wang, Q.; Wang, X.; Wu, Y. *Photochem. Photobiol.* **2019**, *95*, 895−900.

(27) Zhou, J.; Lai, W.; Zhuang, J.; Tang, J.; Tang, D. *ACS Appl. Mater. Interfaces* **2013**, *5*, 2773−2781.

(28) Bao, T.; Fu, R.; Wen, W.; Zhang, X.; Wang, S. *ACS Appl. Mater. Interfaces* **2020**, *12*, 2087−2094.

(29) Liu, S.; Yu, X.; Wang, J.; Liu, D.; Wang, L.; Liu, S. *Anal. Chem.* **2020**, *92*, 9764−9771.

(30) Li, J.; Mo, F.; Guo, L.; Huang, J.; Lu, Z.; Xu, Q.; Li, H. *Sens. Actuators, B* **2021**, *328*, No. 129032.

(31) Zhang, S.; Wang, L.; Liu, C.; Luo, J.; Crittenden, J.; Liu, X.; Cai, T.; Jili, Y.; Pei, Y.; Liu, Y. *Water Res.* **2017**, *121*, 11−19.

(32) Xu, Y.; Schoonen, M. *Am. Mineral.* **2000**, *85*, 543−556.

(33) Hao, Q.; Shan, X.; Lei, J.; Zang, Y.; Yang, Q.; Ju, H. *Chem. Sci.* **2016**, *7*, 774−780.

(34) Zheng, Y. N.; Liang, W. B.; Xiong, C. Y.; Zhuo, Y.; Chai, Y. Q.; Yuan, R. *Anal. Chem.* **2017**, *89*, 9445−9451.

(35) Zhang, X.; Ding, S. N. *ACS Sens.* **2016**, *1*, 358−365.

(36) Zheng, J.; Wang, J.; Song, D.; Xu, J.; Zhang, M. *ACS Appl. Nano Mater.* **2020**, *3*, 3449−3458.

(37) Su, S.; Li, J.; Yao, Y.; Sun, Q.; Zhao, Q.; Wang, F.; Li, Q.; Liu, X.; Wang, L. *ACS Appl. Bio Mater.* **2019**, *2*, 292−298.

(38) Ma, X.; Wang, Z.; He, S.; Chen, C.; Luo, F.; Guo, L.; Qiu, B.; Lin, Z.; Chen, G.; Hong, G. *ACS Sens.* **2019**, *4*, 2375−2380.

(39) Qiu, Z.; Shu, J.; Liu, J.; Tang, D. *Anal. Chem.* **2019**, *91*, 1260−1268.

(40) Qiu, Z.; Shu, J.; Tang, D. *Anal. Chem.* **2018**, *90*, 12214−12220.

(41) Yang, R.; Zou, K.; Zhang, X.; Du, C.; Chen, J. *Chem. Commun.* **2019**, *55*, 8939−8942.

(42) Meng, L.; Li, Y.; Yang, R.; Zhang, X.; Du, C.; Chen, J. *Chem. Commun.* **2019**, *55*, 2182−2185.

(43) Yang, R.; Zou, K.; Zhang, X.; Du, C.; Chen, J. *Biosens. Bioelectron.* **2019**, *132*, 55−61.

(44) Meng, L.; Xiao, K.; Zhang, X.; Du, C.; Chen, J. *Sens. Actuators, B* **2020**, *305*, No. 127480.